1 Title page

Title:

Longitudinal 19F magnetic resonance imaging of brain oxygenation in a mouse model of vascular cognitive impairment using a cryogenic radiofrequency coil

Authors:

Ahmed A Khalil[1,2,3], Susanne Mueller[1,4], Marco Foddis[1], Larissa Mosch[1], Janet Lips[1], Ingo Przesdzing[1], Sebastian Temme[5], Ulrich Flögel[5], Ulrich Dirnagl[1,4,6], Philipp Boehm-Sturm[1,4]

Affiliations/addresses:

1 Charité – Universitätsmedizin Berlin, corporate member of Freie Universität Berlin, Humboldt-Universität zu Berlin, and Berlin Institute of Health, Department of Experimental Neurology and Center for Stroke Research Berlin

2 Max Planck Institute for Human Cognitive and Brain Sciences, Department of Neurology, Leipzig, Germany

3 Humboldt-Universität zu Berlin, Berlin School of Mind and Brain, Berlin, Germany

4 Charité – Universitätsmedizin Berlin, NeuroCure Cluster of Excellence and Charité Core Facility 7T Experimental MRIs

5 Experimental Cardiovascular Imaging, Molecular Cardiology, Heinrich-Heine-University of Düsseldorf

6 Berlin Institute of Health (BIH), Berlin, Germany

Contact details of corresponding author:

Center for Stroke Research Berlin

Charité Universitätsmedizin Berlin

Campus Benjamin Franklin

Hindenburgdamm 30

12200

Berlin, Germany

ahmed-abdelrahim.khalil@charite.de

Acknowledgments:

The authors thank Dr. med. Esmeralda Heiden and Christa Josties for their valuable assistance in establishing the histology protocol used in this study.

This work was supported by the Stiftung Charité (BIH_PRO_317), the DFG Cluster of Excellence NeuroCure (Exc 257), SFB 1116, DFG grants FL 303/6-1 / TE 1209/1-1, and the Federal Ministry of Education and Research (BMBF; 01EO0801, Center for Stroke Research Berlin). Funders played no role in the design, analysis, or reporting of this study.

2 Abstract

Introduction: We explored the use of a perfluoro-15-crown-5 ether nanoemulsion (PFC) for measuring tissue oxygenation using a mouse model of vascular cognitive impairment.

Methods: Seventeen C57BL/6 mice underwent stereotactic injection of PFC coupled to a fluorophore into the striatum and corpus callosum. Combined 1H/19F magnetic resonance imaging (MRI) to localize the PFC and R_1 mapping to assess pO_2 were performed. The effect of gas challenges on measured R_1 was investigated. All mice then underwent bilateral implantation of microcoils around the common carotid arteries to induce global cerebral hypoperfusion. 19F-MRI and R_1 mapping were performed one day, one week, and four weeks after microcoil implantation. In vivo R_1 values were converted to pO_2 through in vitro calibration. Tissue reaction to the PFC was assessed through ex-vivo immunohistochemistry of microglial infiltration.

Results: R_1 increased with increasing oxygen concentrations both in vitro and in vivo and the strength of the 19F signal remained largely stable over four weeks. In the two mice that received all four scans, tissue pO_2 decreased after microcoil implantation and recovered four weeks later. We observed infiltration of the PFC deposits by microglia.

Discussion: Despite remaining technical challenges, intracerebrally injected PFC is suitable for monitoring brain oxygenation in vivo.

Keywords:

Oxygenation, vascular cognitive impairment, 19F-MRI, perfluoro-15-crown-5-ether

3 Introduction

A deficit in tissue oxygenation is a central mechanism of tissue damage in cerebrovascular diseases. In patients and animal models, techniques are available to assess blood flow, local oxygen consumption, and changes in blood oxygenation using magnetic resonance imaging and positron emission tomography [1]. Although measuring these processes is undoubtedly useful, their pathophysiological interpretation is complex (particularly when measured alone) as they are affected by many factors in addition to tissue oxygenation. Methods for directly and non-invasively measuring tissue oxygen concentration, on the other hand, are lacking.

19F-MRI has been used extensively in the past for imaging inflammation and for tracking implanted cells [2–5]. In addition to its general advantages, including the virtual absence of endogenous background 19F signal in vivo, 19F-MRI is useful for quantifying tissue oxygenation. Perfluorocarbons dissolve large amounts of molecular oxygen in a manner that is linearly proportional to the surrounding partial pressure of oxygen [6, 7], a property which has been exploited in their use as blood substitutes [8]. Because molecular oxygen (which has two unpaired electrons) is paramagnetic, it linearly increases the longitudinal relaxation rate (R_1) of perfluorocarbons [9]. This allows the partial pressure of oxygen (pO_2) to be calculated from experimentally measured R_1 values when the temperature of the sample is controlled. This relationship holds across a wide range of pO_2 values and has been validated using more invasive oxygenation measurement methods [10–12].

Vascular cognitive impairment (VCI) is a broad term that relates to several brain pathologies involving cognitive decline of vascular origin, such as stroke or small-vessel disease [13]. Global brain hypoperfusion has been shown to model certain features of human VCI such as glial activation and white matter damage in rats [14] and mice [15]. In the microcoil mouse model of

chronic hypoperfusion, we have recently shown a gradual recovery of blood flow accompanied by remodeling of the Circle of Willis [16]. However, it is unknown whether this critically affects brain tissue oxygenation. In such models of chronic cerebrovascular disorders, the ability to quantify tissue brain oxygenation may prove useful for exploring the pathophysiology of the disease, as well as for monitoring the effects of potential interventions.

In this exploratory study, we investigated whether a perfluoro-15-crown-5 ether nanoemulsion (PFC) is suitable for the in vivo longitudinal monitoring of brain tissue oxygenation. We observed the effect of varying inhaled oxygen concentrations and the induction of global cerebral hypoperfusion on the measured tissue pO_2 values. We used a cryogenically cooled 19F surface coil to improve the signal during 19F-MRI. Compared to a previously published cryogenic 19F coil design [17], the hybrid 1H/19F design allows acquisition of morphological 1H images within the same scanning session for localization of the PFC's signal.

4 Methods

4.1 Preparation of the perfluoro-crown ether nanoemulsion

The PFC was prepared as previously reported [2, 18]. In brief, 2.4% (w/w) phospholipid (Lipoid S75, Lipoid AG, Ludwigshafen, Germany) was dispersed in 10 mM phosphate buffer (isotonized with 2.5% glycerol). 20% (w/w) perfluoro-15-crown-5 ether (ABCR, Karlsruhe, Germany) was added to the dispersion and a crude emulsion was formed by high shear mixing (Ultra Turrax TP 18/10; IKA-Werke, Staufen, Germany). High pressure homogenization was performed in 10 cycles at 1000 bar (Avestin Emulsiflex C5, AVESTIN Europe, Mannheim, Germany). Perfluorocarbons were heat-sterilized in glass vials under standard conditions (121 °C, 2 bar, 20 min.) and stored at 4 °C until administration. Average particle size was determined by photon correlation spectroscopy to be 149±15 nm. The Rhodamine labelling was performed as described

previously by incorporation of rhodamine dihexadecanoic phosphatidylethanolamine into the lipid shell [2].

4.2 Animals, Injections, Microcoil implantation

A single group of seventeen male C57BL/6 mice (purchased at 10 weeks of age from Charles River, Germany) were included in this study and housed in a temperature (22±2°C), humidity (55±10%), and light (12/12-hour light/dark cycle) controlled environment. The experiments described here started one week after the mice arrived at the research facility. An overview of the experimental timeline is shown in Figure 1. All animal procedures performed were approved by the Landesamt für Gesundheit und Soziales under license number G0068/12 and conducted according to the German Animal Welfare Act (Tierschutzgesetz, BGBl. I S. 1206, 1313, http://bit.ly/2Qz6K6E) and the institutional guidelines of the Charité Universitätsmedizin Berlin (Tierschutz-Richtlinie der Charité, November 2016, http://bit.ly/2QFOoRJ).

Prior to the experiments, the stereotactic injection protocol was tested on a healthy mouse to optimize the targeting of the striatum and corpus callosum bilaterally (Figure 1). The mice were anesthetized with 2% isoflurane (Forene, AbbVie Inc., USA), placed into a stereotaxic frame, and the following coordinates were targeted (in mm relative to the bregma): anteroposterior (AP) = +0.5, mediolateral (ML) = -2 (left hemisphere) and AP = +0.5, ML = +2 (right hemisphere). For both hemispheres, the needle (attached to a Hamilton 701 RN 10µL syringe, Hamilton Bonaduz AG, Switzerland) was advanced to dorsoventral (DV) = -4 and then slowly pulled up to DV = -3, where 1µL of the Rhodamine-coupled PFC [19] was injected at a rate of 500 µL/min (striatum). The needle was then pulled up further to DV -1.2, where 1µL of PFC was again injected (corpus callosum). Bubivacain was applied to the wound after the procedure for pain relief.

Four weeks later, global cerebral hypoperfusion was induced in all mice (n=17) by wrapping non-magnetic, surgical-grade steel microcoils with an inner diameter of 160 μm and a length of 2.5 mm (Shannon Coiled Springs Limited, Limerick, Ireland) around the left common carotid artery (Supplementary Figure 1) [15]. Twenty-four hours after the first implantation, an identical microcoil was wrapped around the right common carotid artery in all mice. This two-stage implantation is a refinement of the original method that reduces post-procedure mortality [16]. In this study, the "microcoil implantation" timepoint refers to the day on which the second microcoil was implanted. The operations were performed under 1.2 – 1.5% isoflurane anesthesia (Forene, AbbVie Inc., USA) with the mice breathing a mixture of 70% N_2O and 30% O_2.

4.3 Imaging

All imaging was performed on a 7T BioSpec MR scanner using a hybrid cryogenic 19F surface/room temperature 1H saddle coil (Bruker, Ettlingen, Germany). The mice were anesthetized prior to imaging with 2% inhaled isoflurane (Forene, AbbVie Inc., USA) and maintained on about 1.5% (adjusted to keep vital signs within normal range) while breathing a mixture of 70% N_2O and 30% O_2. We monitored respiration (using a pneumatic pillow), temperature (using a rectal probe), and pulse oximetry (using a probe placed on the mouse's hind paw) throughout the imaging session using MR compatible equipment (Small Animal Instruments Inc., Stony Brook, NY, USA). During testing, we noted that the pulse oximetry device caused an imaging artifact on the 19F scans (stripes due to noise in the 19F frequency range), and so we turned off the pulse oximetry when the 19F sequences were running. Rectal temperature was maintained at 37 +/- 0.5 °C using a water bath connected to a heating mechanism on the animal holder.

We acquired T2-weighted TurboRARE 1H (TR= 3500 ms, $\Delta TE/TE_{effective}$=11 ms/33 ms, 6 averages, FOV [mm^2] = 19.2 x 19.2, matrix = 128 x 128, 16 slices, slice thickness = 1 mm, RARE factor=8, bandwidth=34722 Hz, acquisition time = 5 min 36 s) and 19F (TR=1000 ms, TE = 5 ms, 128 averages, FOV [mm^2] = 19.2 x 19.2. matrix = 48 x 48, 8 slices, slice thickness = 2 mm, RARE factor=16, bandwidth=20 kHz, acquisition time = 6 min 24 s) images. 19F R_1 mapping was performed using a flow-sensitive alternating inversion recovery echo planar imaging (FAIR-EPI) sequence (TR= 5000 ms, TE= 9 ms, inversion times [ms] = (25, 400,800, 1200, 1600), 20 averages, FOV [mm] = 19.2 x 19.2, matrix=48 x 48, single coronal slice, slice thickness=6 mm, acquisition time = 12 min 1 s) with adiabatic inversion pulses (6.8 ms duration, 10 kHz bandwidth, calculated shape) to maximize inversion efficiency. A narrow excitation/refocusing radiofrequency pulse bandwidth of 2.2 kHz was used to minimize artifacts from isoflurane. The FAIR-EPI slice was positioned in a location corresponding to the PFC injection site in each mouse. In the day -7 timepoint (one week before microcoil implantation), the R_1 mapping was repeated for control experiments with the mice inhaling three gas mixtures with oxygen concentrations of 30%, 60%, and 100%.

4.4 In vitro calibration

Six NMR tubes, each containing 700 μL of the PFC were continuously bubbled for 20 minutes with the following gas mixtures: 100% N_2, 12.5% O_2 + 87.5% N_2, 25% O_2 + 75% N_2, 50% O_2 + 50% N_2, 75% O_2 + 25% N_2, 100% O_2 and secured with an air-tight seal using Parafilm (Bemis, USA). The concentration of oxygen in the gas mixture that was bubbled through each tube was converted to partial pressure (in mmHg) for further analysis. Another NMR tube containing the PFC was prepared without bubbling (referred to here as “Air”). The temperature of the samples was maintained at 37 (+/- 0.5) °C during scanning using a water bath connected to a heating blanket. Imaging of the NMR tubes included a localizer and the same FAIR-EPI sequence used

for the in vivo scans. The interval between the end of bubbling and the start of the FAIR-EPI scan was fixed at about 15 minutes for each sample.

4.5 Image processing

The FAIR-EPI images of the in vitro and in vivo data were smoothed with a 0.3 mm Gaussian kernel and an SNR mask was created, composed of voxels with signal at least 5 times higher than the standard deviation of the image intensity in a region-of-interest outside the brain. R_1 fitting was performed on the FAIR-EPI images using the following 3-parameter model accounting for inversion efficiency variations using a custom MATLAB script [20]:

$$S(TI) = |a \cdot (1 - 2b \cdot e^{-TI \cdot R_1})|$$

Here, *S(TI)* refers to the signal intensity at inversion time *TI*, *a* denotes the equilibrium signal, and *b* the inversion efficiency.

For the in vivo data, this was done either on a voxel-by-voxel basis or by fitting the mean FAIR-EPI signal within the SNR >5 mask (the results of both strategies are reported). R_1 values were converted to pO_2 for the in vivo data using the regression equation derived from the in vitro calibration.

4.6 Histology

The mice were euthanized with ketamine-xylazine and transcardially perfused with 4% paraformaldehyde (PFA) for fixation, followed by brain dissection and placement of the brains in PFA for 24 hours, and then in 30% sucrose for 3 days after washing with phosphate-buffered saline (PBS). The brains were frozen at -80 °C and later sliced into 20 µm-thick coronal sections on a cryostat.

The sections were blocked with phosphate-buffered saline (PBS) for 2 hours at room temperature and then with anti-ionized calcium-binding adapter molecule 1 (Iba1) antibody (1:1,000, FUJIFILM Wako Chemicals GmbH, Neuss, Germany) in blocking buffer (1% bovine serum albumin) overnight at 4 °C. They were then washed with PBS and incubated with Alexa Fluor 488 anti-rabbit IgG (1:200, Invitrogen ThermoFisher Scientific, USA) in blocking buffer for 2 hours at room temperature and washed again with PBS. They were then incubated with 4',6-diamidino-2-phenylindole (DAPI, Sigma-Aldrich, USA) for 3 minutes and finally washed with washing solution and distilled water. Fluorescent widefield imaging was performed on a Leica DMi8 microscope, equipped with a Leica DFC3000 G CCD camera (Leica Microsystems GmbH, Wetzlar, Germany).

4.7 Statistical analysis and data availability

All imaging data and analysis scripts are available on Github (https://github.com/ahmedaak/19F_VCI_pOLD_magma). Statistical analysis and data visualization were done in R version 3.4.3 [21] and microscopy images were edited using ImageJ version 1.49 [22]. The experimental unit for all analyses is a single mouse or NMR tube, with three repeated measurements being made on each eligible mouse (n=4) for the gas challenge experiments (i.e. mice that received all three gas challenges and where the R_1 fitting for all three measurements were successful at this timepoint) and four repeated measurements being made on each eligible mouse (n=2) for longitudinal pO_2 monitoring (i.e. mice that received scans at each timepoint and where the R_1 fitting was successful at every timepoint). The relationship between R_1 and pO_2 measured in vitro was determined using linear least squares regression. In this exploratory study no test statistics, blinding, randomization, or formal sample size calculation were performed.

5 Results

5.1 In vitro pO_2 calibration

R_1 fitting was performed using the mean FAIR-EPI signal from the SNR >5 mask for each NMR sample tube. The resulting relationship between R_1 (1/s) and pO_2 (mmHg) is given by:

$$R_1 = 0.4251 + 0.002124[pO_2]$$

The 95% confidence intervals are 0.00177 – 0.00248 (standard error = 0.00014) for the slope and 0.2835 – 0.5668 (standard error = 0.055) for the intercept (adjusted R-squared = 0.98, F = 237.1, $p = 2.096 \times 10^{-5}$, Figure 3).

The coefficients of variation of R_1 in the in vitro samples were 0.04 (0% O_2), 0.08 (12.5% O_2), 0.06 (Air), 0.05 (25% O_2), 0.08 (50% O_2), 0.02 (75% O_2), and 0.02 (100% O_2).

5.2 Intracerebrally injected PFC is stable over time in vivo

One of the investigators (A.K.) visually assessed the SNR maps of the 19F-T2-weighted images (superimposed on the 1H-T2-weighted images) at day -7 (prior to microcoil implantation). The mice were thus classified as having either good (n=4), sufficient (n=3), low (n=5), or no (n=5) signal based on the conspicuity of the 19F signal and whether or not it was in the expected location. Figure 2 and Supplementary Table 1 show the results of this classification (examples shown in Supplementary Figure 2) as well as the experiments and analyses performed on each mouse. R_1 fitting and pO_2 calculation were only performed in mice with good or sufficient signal at baseline (day -7). In some of these mice and at certain timepoints (see Supplementary Table 1), the R_1 fitting failed in spite of this. Mice with failed R_1 fitting at any timepoint were excluded from the final pO_2 analysis.

In the mice that were scanned at all four timepoints (n=8, corresponding to row B of Figure 2), the FAIR-EPI integrated SNR (the mean SNR value in the SNR mask multiplied by the number

of voxels with SNR > 5) was stable over time in most of the mice (Figure 5). Exceptions were M13 and M15, where the PFC was inadvertently injected into the ventricle (Supplementary Figure 3).

5.3 Stereotactic PFC injection results in microglia accumulation

Using an antibody which detects a calcium-binding protein specifically expressed in microglia (Iba1) [23], we observed accumulation of microglia at the sites of the Rhodamine-coupled PFC deposits (Figure 4). This was visible a week before the mice underwent microcoil implantation (timepoint -7, three weeks after injection of the PFC), a week after microcoil implantation (timepoint 7), and four weeks after microcoil implantation (timepoint 28).

5.4 Effects of inhaled O_2 on PFC R_1 values in vivo

As an in vivo positive control, we repeatedly measured R_1 values with the mice inhaling gradually increasing oxygen concentrations. The distribution of voxelwise R_1 values at the timepoint before microcoil implantation (day -7) showed the expected pattern of increase in R_1 with increasing inhaled oxygen concentrations. This is shown for a single mouse in Figure 6B. Figure 6A shows the average raw FAIR-EPI signal within the SNR mask for each oxygen concentration in the same mouse. Figure 6C shows the mean R_1 values in the SNR mask for all mice with good 19F T2 signal visibility who received the gas challenges (n=4, corresponding to row A of Figure 2).

5.5 PFC R_1 mapping of pO_2 changes over time

In the two mice with good/sufficient signal who were imaged at all four timepoints (-7, 1, 7, and 28 – corresponding to row C of Figure 2), R_1 mapping revealed a large decrease in pO_2 after implantation of the microcoils, followed by a recovery to baseline 4 weeks later (Figure 7A). The spatial pO_2 maps across the study timepoints are shown for M08 in Figure 7B.

6 Discussion

Several perfluorocarbons can be emulsified with lipids and used for 19F-MRI [24]. However, the unique properties of perfluoro-15-crown-5 ether nanoemulsions (PFCs) make them particularly suitable for long-term in vivo use. They are fluorine-rich compounds that provide relatively high signal (with 20 fluorine nuclei per molecule), have a very long biological half-life [24], and a 19F spectrum with a single resonance well separated from that of isoflurane, a commonly used inhalational anesthetic in preclinical research [25].

PFCs have been used extensively in the brain for cell tracking, monitoring intracellular oxygenation in tumors, and detection of inflammation [2–5]. However, they have until now not been investigated for non-invasive imaging of pO_2 in brain ischemia. Therefore, the overall aim of this study was to characterize the use of a PFC for longitudinal monitoring of tissue oxygenation in cerebrovascular disorders. For this purpose, we used a dual 1H/19F cryogenically cooled MR radiofrequency coil. Cryogenic coils improve SNR by a factor of 2–3 (depending on the distance from the coil) compared to room-temperature coils [26], potentially improving PFC detection.

We found that the 19F-MRI signal from an intracerebrally injected PFC is largely stable in the first 6 weeks after intracerebral injection and responded to changes in O_2 levels in vitro and in vivo in a manner consistent with that of an oxygenation sensor. This is consistent with the chemically inert nature of the PFC and with previous longitudinal studies using intramuscular PFC injections [27]. This persistent stability of the PFC is advantageous in preclinical studies where long-term follow-up is desired, either with the aim of studying the pathophysiology of a disease, or for investigating the effects of potential therapeutic interventions. For clinical translation, however, perfluorocarbons with shorter half-lives than PFC would be desirable. A

thorough comparison of the clearance properties of perfluorocarbons in the brain has not yet been done. Such studies would help us balance the suitability of a perfluorocarbon for longitudinal applications with its potential for causing long-term side effects.

The bilateral carotid artery stenosis mouse model shows several pathophysiological and phenotypic features of human vascular cognitive impairment. These include working memory impairment, white matter damage, vascular remodeling indicative of recruitment of collateral flow pathways, and changes in the brain's functional organization [15, 16, 28]. In a very limited sample of two mice, our results show that tissue oxygenation drops following bilateral occlusion of the carotid arteries using microcoils. Tissue oxygenation recovers, apparently to baseline levels, by 4 weeks post-occlusion, a pattern which resembles changes in cerebral blood flow [15, 16] and oxygen consumption in this model [29]. This observation requires confirmation, preferably in studies combining different imaging modalities for measuring these fundamental physiological parameters in the same sample.

Although the pattern of changes in oxygenation over time that we observed in this study is consistent with the pathophysiology of this disease model, the absolute pO_2 values measured were very high (about 90 mmHg). In normal rodent brain tissue, pO_2 values range from about 6 to 35 mmHg, with higher values (60 – 90 mmHg) occurring in close proximity to red blood cells [30–32]. The overestimation in our study may have been caused by the effect of the isoflurane, which can almost double pO_2 through an increase in cerebral blood flow [32]. On the other hand, this overestimation may have been caused by a systematic error due to discrepancies between the measured rectal temperature and the actual brain temperature [33]. Because PFC is particularly sensitive to temperature [34, 35], the presence of such a systematic error cannot be completely ruled out despite careful control of the rectal temperature. Finally, a decrease in pO_2 in the NMR

tubes between the end of bubbling and the 19F-MRI scan could explain the high absolute pO_2 values in vivo, because such a decrease would produce a calibration curve that is less steep than the true curve. However, the relative pO_2 values (i.e. the pattern of changes across time) in this study should be reliable nonetheless.

Another factor affecting the absolute pO_2 values could be imperfect R_1 measurement due to the inhomogeneous B1+ field associated with using a surface coil for radiofrequency transmission. We aimed to minimize this using adiabatic inversion pulses and a three-parameter fitting model. The resulting R_1 values were homogenous across a 5 mm NMR tube containing PFC in the in vitro calibration experiments (with coefficients of variation ranging from 0.02 to 0.08), which indicates that our strategy compensates for this hardware limitation. However, a systematic error in R_1 measurements when going from the in vitro to the in vivo situation can still not be fully excluded.

Although intracerebral PFC injection is relatively invasive, it avoids certain limitations of intravenous injection [33]. These include lower SNR within the brain caused by sequestration of the PFC in the liver and spleen [36] and the preferential delivery of the PFC to areas with adequate tissue perfusion [37, 38]. The latter can be a particularly crucial confounder in models of more localized diseases such as focal ischemia or brain tumors, where the sequestration leads to over-estimation of tissue pO_2 values in hypoperfused areas. This does not occur when the PFC is distributed relatively uniformly through direct tissue injection [39].

It is particularly important in longitudinal studies that the contrast agent be non-toxic in vivo, so as not to bias measurements made over time. Although certain perfluorocarbons such as hexafluorobenzene showed toxic effects in muscle tissue starting about 24 hours after injection, this was not the case with PFC [27], which also showed a good toxicity profile in vitro [40].

Although we observed an accumulation of microglia around the PFC deposits at multiple timepoints in this study, it is unclear from the qualitative and exploratory histology experiments in this study whether this is a reaction to the stereotactic injection itself, the PFC, the Rhodamine, or all of these. Stereotactic injections of saline are associated with accumulation and activation of microglia in the vicinity of the injection site [41–43] and evidence from cell culture experiments suggests that coupling the PFC with a chemically non-inert fluorophore increases cell damage [43] . Further studies should examine the source of the inflammatory reaction observed in this study in more detail and the possible consequences this reaction may have on tissue oxygenation.

Our study also highlights several practical methodological issues that should be taken into account when performing similar studies. The first is the importance of checking the location of the stereotactically injected PFC deposits, facilitated in our study by the use of the dual 1H/19F coil. The main challenges faced when performing stereotactic PFC injections include the anatomical variability between mice, especially around the lateral ventricles, the high viscosity of the emulsion that can lead to variability in injection volumes or (despite taking measures to avoid this) agent leakage during withdrawal of the needle. Indeed, this variability led to high exclusion rates, which is a major limitation of our study. In future studies, acquiring individual anatomical scans before the injections could help in selecting the appropriate stereotactic coordinates.

Another technical issue to be considered is the possibility of image artefacts originating from presumably MR-compatible equipment (in our case the pulse oximetry system). Since noise levels from these devices are generally tested on the 1H frequency range, MR compatibility in the 19F frequency range is not necessarily a given and should be assessed experimentally.

Absolute quantification of brain oxygenation using 19F-MRI after either intracerebral or intravenous injection of PFCs may prove useful for assessing the tissue’s response to novel

treatment interventions in animal models of cerebrovascular disorders. In addition, the method may find future use as a quantitative reference for validating other, less invasive, methods that are currently being developed and which have promising clinical applications [44].

Although some technical challenges remain, as well as unanswered questions about its toxicity to brain tissue in vivo, quantification of brain oxygenation using 19F-MRI of a PFC shows promising characteristics that make it suitable for longitudinal in vivo preclinical studies.

7 Author contributions

Study conception and design: AAK, ST, UF, UD, PB-S

Acquisition of data: AAK, SM, MF, LM, JL, IP, PB-S

Analysis and interpretation of data: AAK, IP, PB-S

Drafting of manuscript: AAK, PB-S

Critical revision: AAK, SM, MF, LM, JL, IP, ST, UF, UD, PB-S

8 References

1. Filippi M (2015) Oxford Textbook of Neuroimaging. doi: 10.1093/med/9780199664092.001.0001

2. Flögel U, Ding Z, Hardung H, Jander S, Reichmann G, Jacoby C, Schubert R, Schrader J (2008) In vivo monitoring of inflammation after cardiac and cerebral ischemia by fluorine magnetic resonance imaging. Circulation 118:140–148.

3. Ruiz-Cabello J, Walczak P, Kedziorek DA, Chacko VP, Schmieder AH, Wickline SA, Lanza GM, Bulte JWM (2008) In vivo "hot spot" MR imaging of neural stem cells using fluorinated nanoparticles. Magn Reson Med 60:1506–1511.

4. Srinivas M, Boehm-Sturm P, Figdor CG, de Vries IJ, Hoehn M (2012) Labeling cells for in vivo tracking using19F MRI. Biomaterials 33:8830–8840.

5. Waiczies H, Lepore S, Drechsler S, Qadri F, Purfürst B, Sydow K, Dathe M, Kühne A, Lindel T, Hoffmann W, Pohlmann A, Niendorf T, Waiczies S (2013) Visualizing brain inflammation with a shingled-leg radio-frequency head probe for 19F/1H MRI. Sci Rep 3:1280.

6. Pittman RN (2011) Regulation of Tissue Oxygenation. Colloq Ser Integr Syst Physiol From Mol to Funct. doi: 10.4199/C00029ED1V01Y201103ISP017

7. Spiess BD (2009) Perfluorocarbon emulsions as a promising technology: a review of tissue and vascular gas dynamics. J Appl Physiol 106:1444–1452.

8. Riess JG, Riess JG (2001) Oxygen carriers ("blood substitutes") - Raison d'etre, chemistry, and some physiology. Chem Rev 101:2797–2919.

9. Parhami P, Fung BM (1983) Fluorine-19 relaxation study of perfluoro chemicals as oxygen carriers. J Phys Chem 87:1928–1931.

10. Jordan BF, Cron GO, Gallez B (2009) Rapid monitoring of oxygenation by 19F magnetic resonance imaging: Simultaneous comparison with fluorescence quenching. Magn Reson Med 61:634–638.

11. Mason RP, Hunjan S, Constantinescu A, Song Y, Zhao D, Hahn EW, Antich PP, Peschke P (2003) Tumor oximetry: comparison of 19F MR EPI and electrodes. Adv Exp Med Biol 530:19–27.

12. Zhao D, Jiang L, Mason RP (2004) Measuring changes in tumor oxygenation. Methods Enzymol 386:378–418.

13. Dichgans M, Leys D (2017) Vascular Cognitive Impairment. Circ Res 120:573–591.

14. Wakita H, Tomimoto H, Akiguchi I, Kimura J (1994) Glial activation and white matter changes in the rat brain induced by chronic cerebral hypoperfusion: an immunohistochemical study. Acta Neuropathol 87:484–492.

15. Shibata M, Ohtani R, Ihara M, Tomimoto H (2004) White matter lesions and glial activation in a novel mouse model of chronic cerebral hypoperfusion. Stroke 35:2598–2603.

16. Boehm-Sturm P, Füchtemeier M, Foddis M, Mueller S, Trueman RC, Zille M, Rinnenthal JL, Kypraios T, Shaw L, Dirnagl U, Farr TD (2017) Neuroimaging Biomarkers Predict Brain Structural Connectivity Change in a Mouse Model of Vascular Cognitive Impairment. Stroke 48:468–475.

17. Waiczies S, Millward JM, Starke L, Delgado PR, Huelnhagen T, Prinz C, Marek D, Wecker

D, Wissmann R, Koch SP, Boehm-Sturm P, Waiczies H, Niendorf T, Pohlmann A (2017) Enhanced Fluorine-19 MRI Sensitivity using a Cryogenic Radiofrequency Probe: Technical Developments and Ex Vivo Demonstration in a Mouse Model of Neuroinflammation. Sci Rep 7:9808.

18. Ebner B, Behm P, Jacoby C, Burghoff S, French BA, Schrader J, Flögel U (2010) Early assessment of pulmonary inflammation by 19F MRI in vivo. Circ Cardiovasc Imaging 3:202–10.

19. Grapentin C, Mayenfels F, Barnert S, Süss R, Schubert R, Temme S, Jacoby C, Schrader J, Flögel U (2014) Optimization of perfluorocarbon nanoemulsions for molecular imaging by 19F MRI. Nanomedicine 268–286.

20. Kowalewski J, Levy GC, Johnson LF, Palmer L (1977) A three-parameter non-linear procedure for fitting inversion-recovery measurements of spin-lattice relaxation times. J Magn Reson 26:533–536.

21. R Core Team (2016) R: A language and environment for statistical computing. R Foundation for Statistical Computing, R Foundation for Statistical Computing, Vienna, Austria.

22. Schneider CA, Rasband WS, Eliceiri KW (2012) NIH Image to ImageJ: 25 years of image analysis. Nat Methods 9:671–675.

23. Ito D, Imai Y, Ohsawa K, Nakajima K, Fukuuchi Y, Kohsaka S (1998) Microglia-specific localisation of a novel calcium binding protein, Iba1. Mol Brain Res 57:1–9.

24. Jacoby C, Temme S, Mayenfels F, Benoit N, Krafft MP, Schubert R, Schrader J, Flögel U (2014) Probing different perfluorocarbons for in vivo inflammation imaging by19F MRI:

Image reconstruction, biological half-lives and sensitivity. NMR Biomed 27:261–271.

25. Constantinides C, Maguire ML, Stork L, Swider E, Srinivas M, Carr CA, Schneider JE (2017) Temporal accumulation and localization of isoflurane in the C57BL/6 mouse and assessment of its potential contamination in19F MRI with perfluoro-crown-ether-labeled cardiac progenitor cells at 9.4 Tesla. J Magn Reson Imaging 45:1659–1667.

26. Baltes C, Radzwill N, Bosshard S, Marek D, Rudin M (2009) Micro MRI of the mouse brain using a novel 400 MHz cryogenic quadrature RF probe. NMR Biomed 22:834–842.

27. Mignion L, Magat J, Schakman O, Marbaix E, Gallez B, Jordan BF (2013) Hexafluorobenzene in comparison with perfluoro-15-crown-5-ether for repeated monitoring of oxygenation using 19F MRI in a mouse model. Magn Reson Med 69:248–254.

28. Jadavji NM, Farr TD, Lips J, Khalil AA, Boehm-Sturm P, Foddis M, Harms C, Füchtemeier M, Dirnagl U (2015) Elevated levels of plasma homocysteine, deficiencies in dietary folic acid and uracil-DNA glycosylase impair learning in a mouse model of vascular cognitive impairment. Behav Brain Res 283:215–226.

29. Temma T, Yamazaki M, Miyanohara J, Shirakawa H, Kondo N, Koshino K, Kaneko S, Iida H (2017) Sequential PET estimation of cerebral oxygen metabolism with spontaneous respiration of 15 O-gas in mice with bilateral common carotid artery stenosis. J Cereb Blood Flow Metab 37:3334–3343.

30. Sakadžić S, Roussakis E, Yaseen MA, Mandeville ET, Srinivasan VJ, Arai K, Ruvinskaya S, Devor A, Lo EH, Vinogradov SA, Boas DA (2010) Two-photon high-resolution measurement of partial pressure of oxygen in cerebral vasculature and tissue. Nat Methods 7:755–759.

31. Zhang C, Bélanger S, Pouliot P, Lesage F (2015) Measurement of local partial pressure of oxygen in the brain tissue under normoxia and epilepsy with phosphorescence lifetime microscopy. PLoS One 10:e0135536.

32. Lyons DG, Parpaleix A, Roche M, Charpak S (2016) Mapping oxygen concentration in the awake mouse brain. Elife. doi: 10.7554/eLife.12024

33. Robinson SP, Griffiths JR (2004) Current issues in the utility of 19F nuclear magnetic resonance methodologies for the assessment of tumour hypoxia. Philos Trans R Soc Lond B Biol Sci 359:987–96.

34. Dardzinski BJ, Sotak CH (1994) Rapid tissue oxygen tension mapping using 19F inversion???recovery echo???planar imaging of P erfluoro???15 ???crown???5???ether. Magn Reson Med 32:88–97.

35. Yu JX, Cui W, Zhao D, Mason RP (2008) Non-Invasive Physiology and Pharmacology Using19F Magnetic Resonance. Fluor. Heal. Elsevier, pp 197–276

36. Mason RP, Antich PP, Babcock EE, Gerberich JL, Nunnally RL (1989) Perfluorocarbon imaging in vivo: A 19F MRI study in tumor-bearing mice. Magn Reson Imaging 7:475–485.

37. Mason RP, Antich PP, Babcock EE, Constantinescu A, Peschke P, Hahn EW (1994) Non-invasive determination of tumor oxygen tension and local variation with growth. Int J Radiat Oncol Biol Phys 29:95–103.

38. Mcintyre DJO, McCoy CL, Griffiths JR (1999) Tumour oxygenation measurements by f-19 magnetic resonance imaging of perfluorocarbons. Curr Sci 76:753–762.

39. Baete SH, Vandecasteele J, De Deene Y (2011) 19F MRI oximetry: Simulation of

perfluorocarbon distribution impact. Phys Med Biol 56:2535–2557.

40. Srinivas M, Cruz LJ, Bonetto F, Heerschap A, Figdor CG, de Vries IJM (2010) Customizable, multi-functional fluorocarbon nanoparticles for quantitative in vivo imaging using 19F MRI and optical imaging. Biomaterials 31:7070–7077.

41. Xue M, Del Bigio MR (2000) Intracerebral injection of autologous whole blood in rats: Time course of inflammation and cell death. Neurosci Lett 283:230–232.

42. Aucott H, Lundberg J, Salo H, Klevenvall L, Damberg P, Ottosson L, Andersson U, Holmin S, Erlandsson Harris H (2018) Neuroinflammation in Response to Intracerebral Injections of Different HMGB1 Redox Isoforms. J Innate Immun 10:215–227.

43. Boehm-Sturm P, Aswendt M, Minassian A, Michalk S, Mengler L, Adamczak J, Mezzanotte L, Löwik C, Hoehn M (2014) A multi-modality platform to image stem cell graft survival in the naïve and stroke-damaged mouse brain. Biomaterials 35:2218–2226.

44. Christen T, Bolar DS, Zaharchuk G (2013) Imaging brain oxygenation with MRI using blood oxygenation approaches: Methods, validation, and clinical applications. Am J Neuroradiol 34:1113–1123.

9 Figures

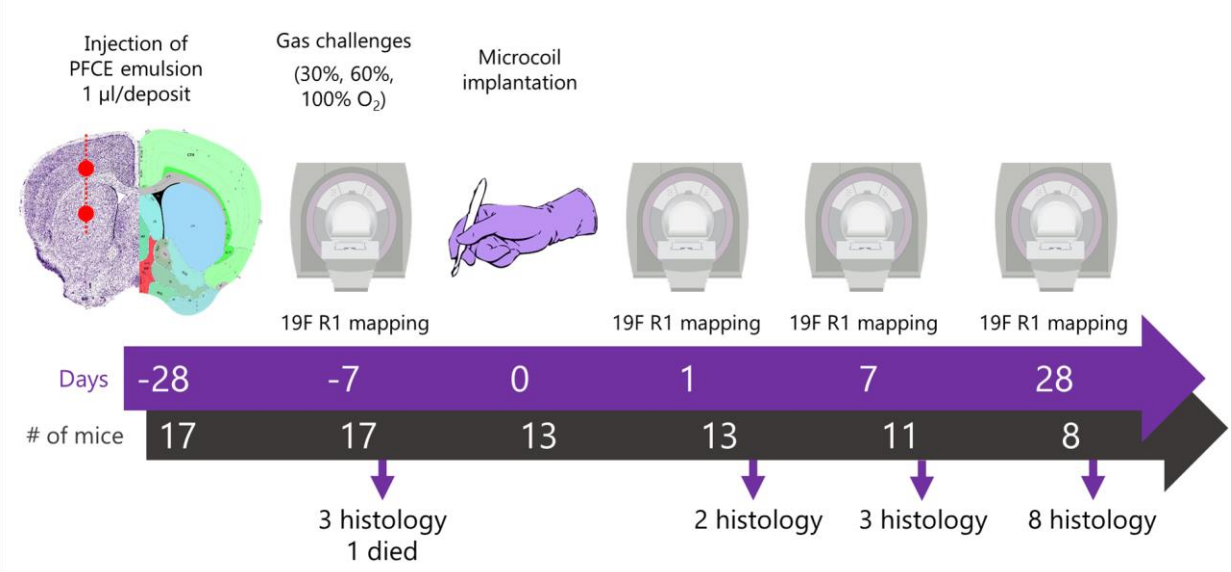

Figure 1 – Overview of the study design. Stereotactic injections took place when the mice were 11 weeks old. The red line on the brain slice to the left shows the path of the injection needle, with sites of PFC deposition marked with a red circle. Days are shown on the figure relative to the microcoil implantation timepoint (day 0 refers to the day where the bilateral carotid artery stenosis surgery was completed, i.e. after the second microcoil was implanted). All mice underwent microcoil implantation. One mouse (M02) died during the first post-surgery scan session (day 1).

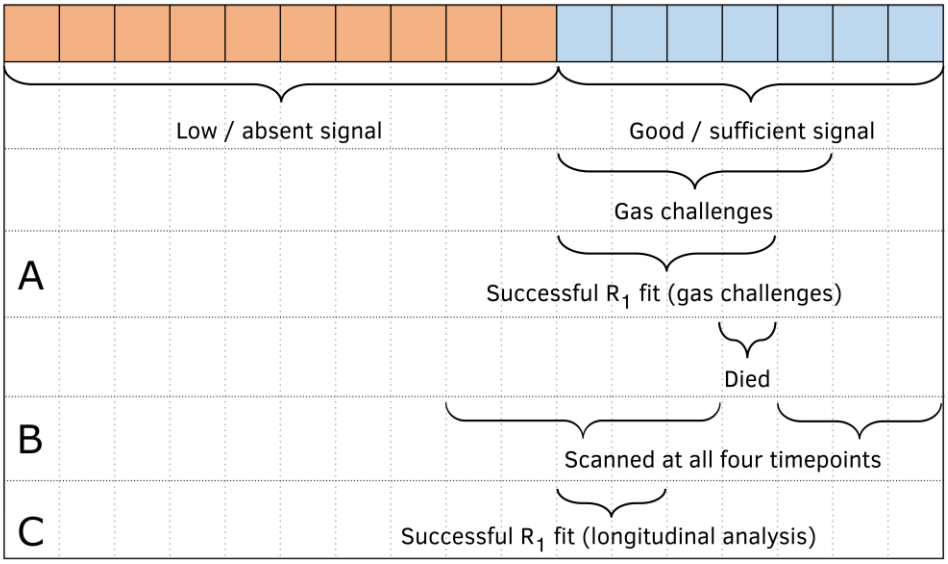

Figure 2 – Overview of the number of mice used for the different analytical steps. Each individual square in the top row represents one mouse initially included in the study. The letters on the left represent analytical steps undertaken at different timepoints – A refers to the analysis of the effects of inhaled O_2 concentration on R_1, B refers to the analysis of the stability of the 19F signal, and C refers to the analysis of longitudinal changes in pO_2.

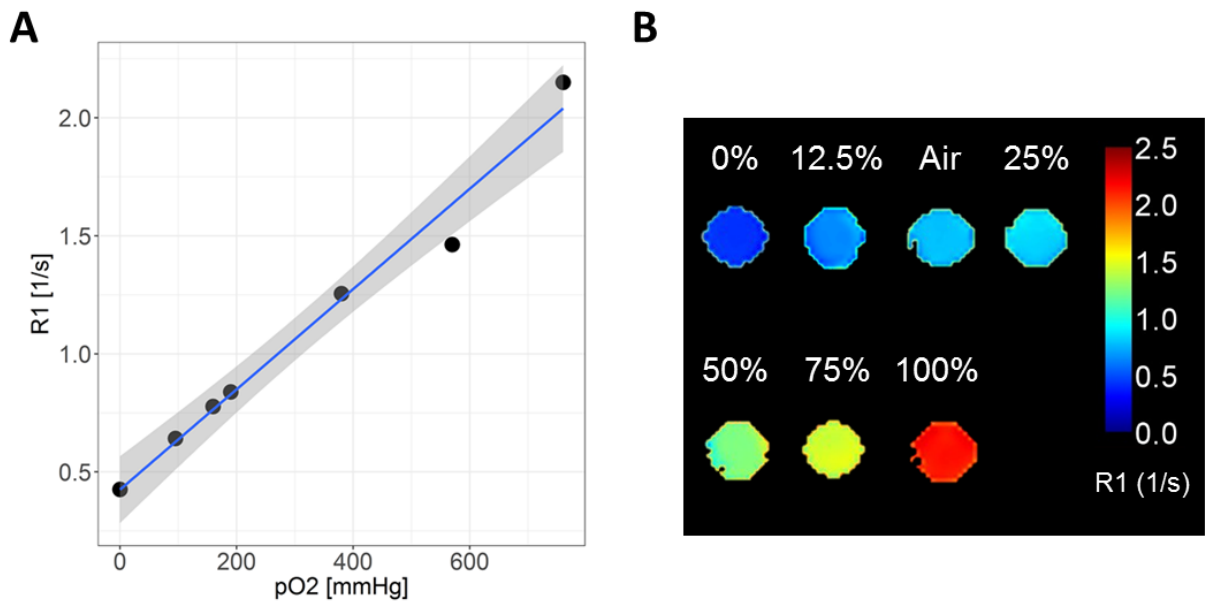

Figure 3 – A) Calibration curve showing the relationship between R_1 and pO_2 (7T scanner, 37 +/- 0.5 °C). Linear least squares regression slope = 0.002124, intercept = 0.4251, R^2 = 0.98 (the shaded area around the regression line is the 95% confidence interval). B) R_1 maps of the NMR tubes used for in vitro R_1/pO_2 calibration.

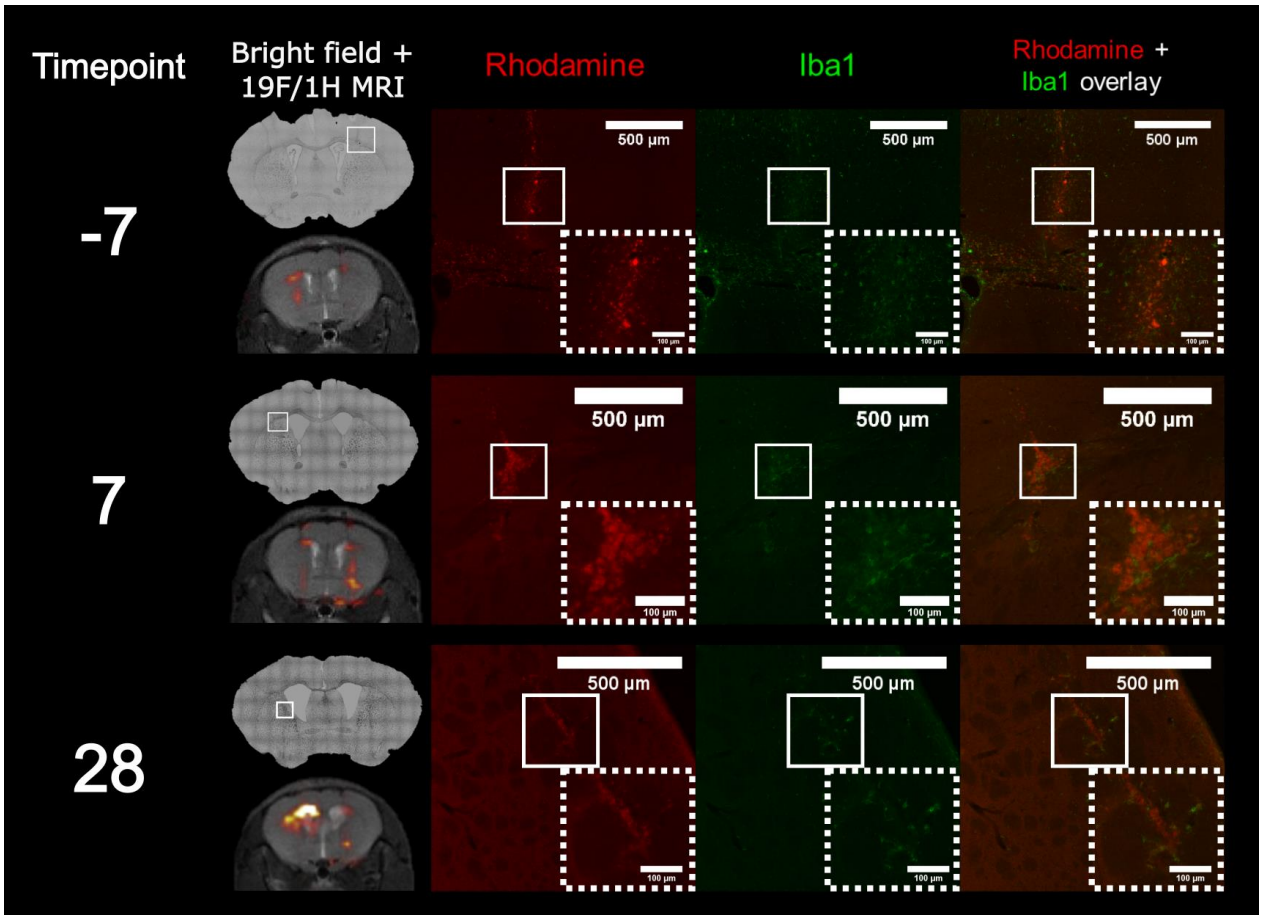

Figure 4 – Fluorescence microscopy of the perfluoro-15-crown-5 ether nanoemulsion (PFC), labelled with Rhodamine (red), and microglia-specific ionized calcium binding adaptor molecule 1 (Iba1) immunofluorescent staining (green). Bright field microscopy images give an overview of the regions depicted in the fluorescence microscopy images. Boxes with dashed lines in the fluorescence microscopy images show zoomed-in images of the regions in the white boxes for better visualization of the morphology of the Iba1-positive cells and their spatial relationship to the PFC. This is shown for three different mice that were sacrificed at timepoints -7 (M01, top row), 7 (M11, middle row), and 28 (M03, bottom row).

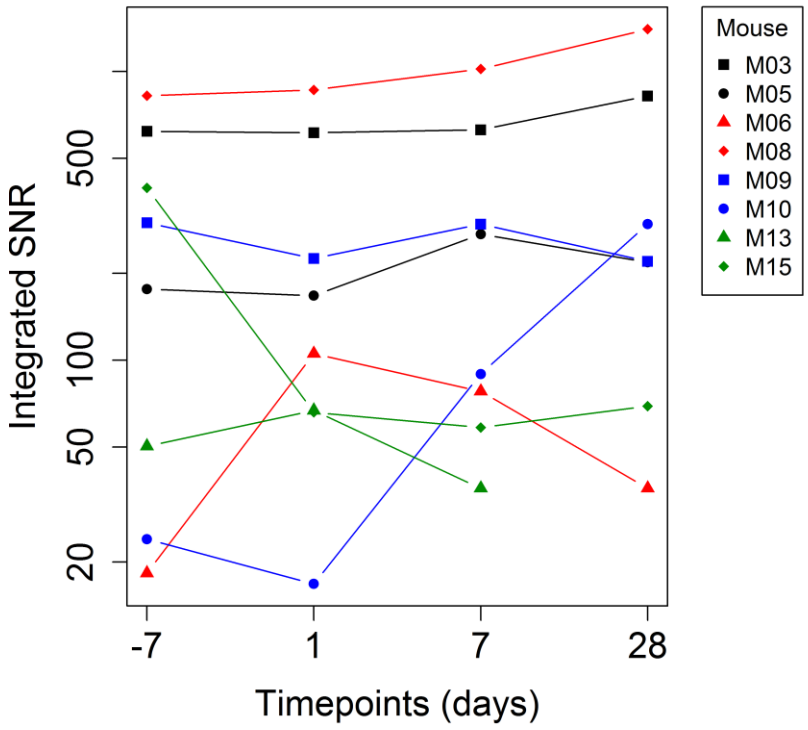

Figure 5 – Integrated SNR of the 19F FAIR-EPI sequence for the mice (n=8) who received scans on all four of the study timepoints. Note that the y-axis is on a logarithmic scale (at day 28, M13 had an integrated SNR of 0 [data point not shown]).

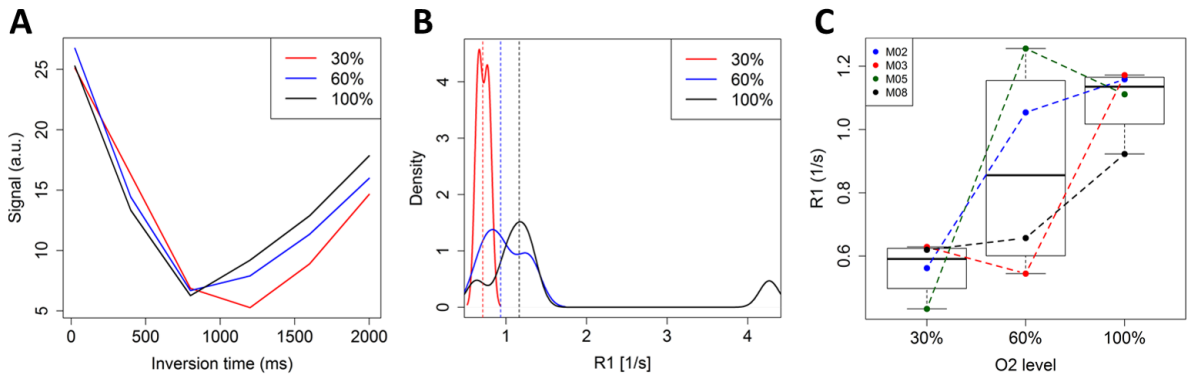

Figure 6 – A) Changes in the raw FAIR-EPI signal (mean signal within the SNR > 5 mask) with different inversion times with the mouse (M05) breathing different gas mixtures (30%, 60%, and 100% O_2, with N_2O forming the remainder). B) Voxelwise distribution of R_1 values in the SNR > 5 mask of M05 during the gas challenges. C) Boxplots showing R_1 values derived from the mean FAIR-EPI signal in each of the mice (n=4) who received the gas challenges at day -7.

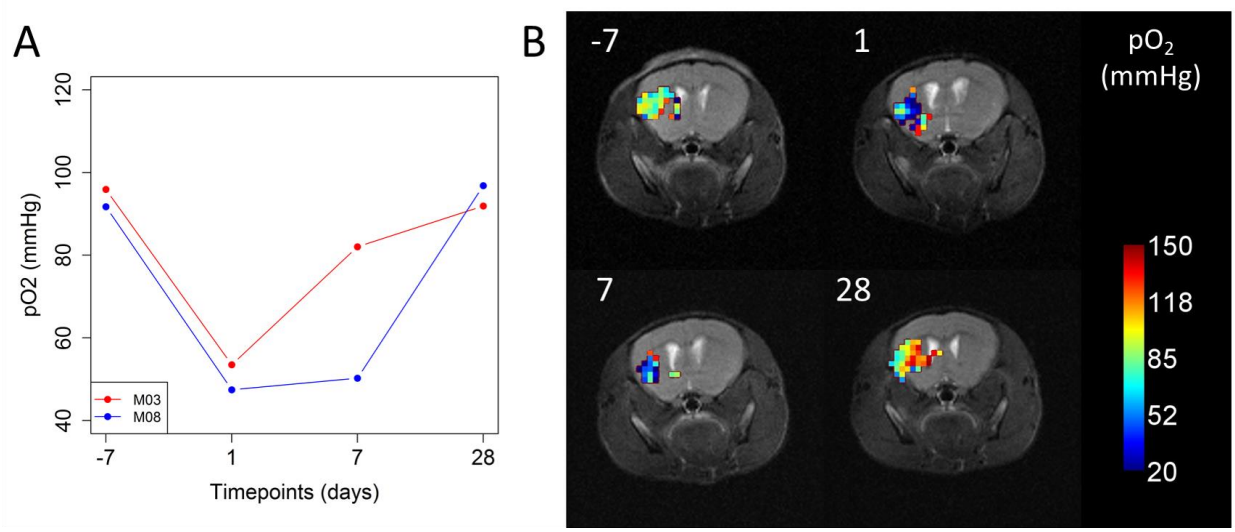

Figure 7 – A) Changes in pO_2, derived from fitting the mean FAIR-EPI signal in the SNR > 5 mask, over the study timepoints show a drop in pO_2 after the microcoil implantation, followed by gradual recovery by day 28. B) Spatial pO_2 maps for M08 showing the same longitudinal pattern of changes in oxygenation.